AIAA JOURNAL
Vol. 34, No. 11, November 1996

Rayleigh Scattering Technique for Simultaneous Measurements of Velocity and Thermodynamic Properties

Gregory S. Elliott* and Mo Samimy†
Ohio State University, Columbus, Ohio 43210

A molecular-filter-based flow diagnostic technique termed filtered angularly resolved Raleigh scattering is used to measure velocity, density, and temperature simultaneously. The technique uses an anamorphic optical system to record the Rayleigh scattered signal viewed at different angles and focused onto an intensified charge-coupled device camera. The experimentally obtained intensity vs viewing angle profiles are then combined with a well-known computational model to solve for the velocity, density, and temperature. The technique was used in a supersonic axisymmetric jet operated at a variety of flow conditions from Mach 1 to 2.3. The measured velocity and thermodynamic properties are compared with the theoretical values in the core of the jet. The measured values are within 11% for the velocity and 7% for the other thermodynamic properties. The error levels agree with the level of uncertainty that is calculated for the system. Methods of reducing the uncertainty and improving the technique also are discussed.

Nomenclature

A_i	= transmission
f	= frequency
$f(u_i)$	= measured quantity as a function of independent variables
f_0	= laser frequency
I	= intensity
I_0	= reference intensity
K	= magnitude of the scattered wave vector
k	= Boltzmann constant
$\boldsymbol{k}_0$	= incident unit light wave vector
$\boldsymbol{k}_s$	= observed unit light wave vector
M	= molecular weight
M_e	= equivalent Mach number
P	= pressure
P_0	= stagnation pressure
$R(x, y)$	= nondimensional Rayleigh scattering profile
r	= Rayleigh scattering profile in terms of dimensional quantities
T	= temperature
T_0	= stagnation temperature
U	= streamwise velocity
$\boldsymbol{V}$	= velocity vector
V_0	= most probable molecular velocity
x	= dimensionless frequency
x_s	= streamwise direction
y	= y parameter, ratio of the collision frequency to the acoustic spatial frequency
y_s	= lateral direction
z_s	= spanwise direction
α	= viewing angle
Δf_D	= Doppler shift
Δu_f	= overall uncertainty of measured quantity (dependent variable)
Δu_i	= uncertainty of independent variable
λ	= wavelength of laser
θ	= angle between the incident and scattered wave vectors
ρ	= density

Received June 2, 1995; revision received Aug. 10, 1995; accepted for publication April 29, 1996.

*Postdoctoral Research Associate, Department of Mechanical Engineering; currently Assistant Professor, Department of Mechanical and Aerospace Engineering, Rutgers University, Piscataway, NJ 08855. Member AIAA.

†Professor, Department of Mechanical Engineering. Associate Fellow AIAA.

Introduction

MANY diagnostic techniques are available to the experimentalist for the study of fluid properties in a given flowfield. Traditionally, intrusive techniques such as hot-wire anemometry, pressure probes, and thermocouples are used in flow investigations, but often questions arise as to their effect on the flowfield being measured. Also, the simultaneous measurement of multiple properties is limited using these methods. Optical techniques offer the possibility of measuring fluid properties without disturbing the flow as well as measuring multiple properties simultaneously.

Recently, techniques employing molecular filters to modify the light scattered from particles or molecules in the flowfield offer the possibility of measuring velocity, a single property, or multiple properties in a flowfield simultaneously. The molecular filter is simply a cylindrical optical cell that contains a molecule that has absorption lines within the bandwidth of the laser interrogating the flowfield. The molecular filter is placed in front of the receiving optics to modify the recorded intensity based on the change in frequency of the scattered light. One of the first uses of iodine molecular filters was by Shimizu et al.,[1] who used it to block the narrow scattering of particles in atmospheric measurements of temperature and pressure. Miles et al.[2,3] extended the use of molecular iodine filters to flow diagnostics, a technique that they called filtered Rayleigh scattering (FRS). By using an injection-seeded frequency-doubled Nd:YAG laser ($\lambda = 532$ nm), the linewidth is narrow enough and can be tuned through some of the broadened hyperfine absorption bands of iodine. Using the FRS technique for background suppression, the laser is tuned so that unwanted scattering from walls and windows is absorbed while the Doppler-shifted Rayleigh (or Mie) scattering from particles or molecules in the flowfield is shifted outside the absorption profile. The magnitude of the Doppler shift is given by

$$\Delta f_D = (1/\lambda)(\boldsymbol{k}_s - \boldsymbol{k}_0) \cdot \boldsymbol{V} \tag{1}$$

The FRS flow visualization technique has been used for background suppression in the study of compressible free mixing layers[4] and in the study of boundary layers.[5] In addition to simple flow visualizations, Miles et al.[3] showed that by tuning the laser frequency through the width of the absorption well of the I_2 absorption profile the average thermodynamic state of the flow at each point in the illuminated plane can be obtained.

Another way of obtaining this intensity-vs-frequency profile, which can be compared to the computer model of the Rayleigh scattering, was suggested by Shirley and Winter[6] in a technique that they termed angularly resolved filter Rayleigh scattering. Instead of scanning the laser to vary the frequency, Shirley and Winter used the fact that the Doppler shift changes for different viewing angles. By use of an anamorphic optical system (discussed later), the rays

viewed at different angles are recorded separately onto the intensified charge-coupled device (ICCD) camera elements. By comparing this intensity-vs-viewing angle profile with a computational model of the scattering, measurements have been made of mass flux in the freestream of a supersonic tunnel.

Komine et al.[7] and Meyers[8] used an optically thin iodine filter whose absorption profile exhibited more gradual slopes (relative to the sharp cutoff slopes used in FRS techniques) to discriminate the Doppler shift from Mie scattering of particles seeded into a subsonic flow. By tuning a narrow-linewidth argon ion laser to the 50% absorption position of the iodine profile, a positive Doppler shift results in an increase and a negative Doppler shift results in a decrease in the detected intensity. Using multiple cameras at different angles, Meyers[8] was able to measure three-component average velocity around a delta wing. Similar optically thin absorption filters were used by Smith and Northam[9] to make instantaneous measurements in an axisymmetric jet. One attractive aspect of their system was its ability to record both a reference and a filtered image on a single camera, thus reducing the cost.

Elliott et al.[10] used a multiple-camera technique called filtered planar velocimetry to measure the instantaneous velocities in a compressible mixing layer. In this case, the scattering was provided from condensed water particles and the filter profile was controlled by using nitrogen to pressure broaden the iodine absorption profile. This technique enabled Elliott et al.[10] to tune the profile to the velocity range expected in the flowfield. Also, by use of an optically thick iodine cell, the laser could be tuned to suppress the background scattering while the Doppler-shifted signal is discriminated.

The objective of the molecular filter technique described in this paper, called filtered angularly resolved Rayleigh scattering (FARRS), is the simultaneous measurement of velocity, density, and temperature. Using the ideal gas law, pressure also can be calculated. Following is a description of the FARRS technique, the experimental setup, and results from preliminary measurements. Although this initial investigation was based on obtaining average results to verify the technique, instantaneous measurements can be made using the same technique. The paper concludes with a simple uncertainty analysis, and a presentation of ideas to reduce the error.

Description of FARRS System and Technique

In describing the FARRS system, a brief background on Rayleigh scattering and the calculation of the spectral content of the Rayleigh scattering signal is given. This is followed by a description of the optical components and the scheme to solve for the velocity and the thermodynamic properties from the intensity profile recorded by the camera.

Because the FARRS technique is based on Rayleigh scattering, one needs to understand what flow properties affect the spectral shape of the signal. Unlike scattering from particles (Mie scattering), the shape of the scattering spectrum for molecular Rayleigh scattering is affected by the thermal and acoustic motion of the scattering molecules. The shape of the scattering spectrum is typically parameterized by two variables, the dimensionless frequency x, and the y parameter.[2] The dimensionless frequency is given by

$$x = (2\pi/KV_0)|f - f_0| \tag{2}$$

where $(f - f_0)$ is the frequency difference from line center. The magnitude of the scattered wave vector is given by

$$K = (4\pi/\lambda)\sin(\theta/2) \tag{3}$$

The most probable molecular velocity V_0 is given by

$$V_0 = \sqrt{(2kT/M)} \tag{4}$$

The second parameter is the y parameter, given by

$$y = (P/KV_0\mu) \tag{5}$$

where μ is the viscosity.[2] The y parameter can be written for air as[1]

$$y = 0.2308\left(\frac{T[\mathrm{K}] + 110.4}{T^2[\mathrm{K}]}\right)\left(\frac{P[\mathrm{atm}]\lambda[\mathrm{nm}]}{\sin(\theta/2)}\right) \tag{6}$$

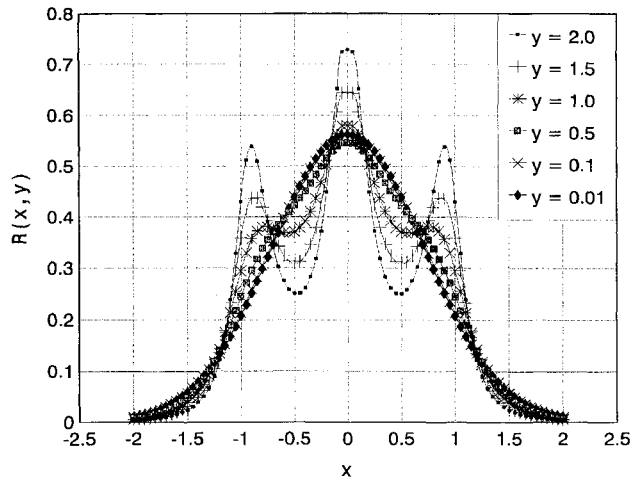

Fig. 1 Molecular Rayleigh scattering profiles for various y parameters.

Figure 1 gives the molecular Rayleigh scattering spectral profile $R(x, y)$ for various y parameters calculated from the model given by Yip and Nelkin[11] and normalized such that

$$\int_{-\infty}^{\infty} R(x, y)\,\mathrm{d}x = 1 \tag{7}$$

For y values greater than 1, Brillouin peaks become signficant; but at lower y values ($y < 0.1$), the scattering is essentially Gaussian.[2] An understanding of these properties is necessary for the use of Rayleigh scattering from molecules in molecular-filter techniques, including FARRS.

Shirley and Winter[6] introduced the idea of an angularly resolved filtered Rayleigh scattering to potentially obtain mass flux measurements in a supersonic wind tunnel. Using an anamorphic optical system (an optical system that has different magnifications along two perpendicular directions), they were able to collect the scattering from different viewing angles and record them onto an ICCD camera. The anamorphic optical system used in the present FARRS experiments is to some degree similar to that of Shirley and Winter[6] and is shown schematically in Fig. 2. This system allows the intensity at different viewing angles to be recorded separately by the ICCD camera. The system utilizes a low f-number photographic lens (i.e., $f/1.4$) so that the viewing half angle is approximately ± 20 deg about the centerline. The field stop placed at the focal point of the photographic lens prevents off-axis light from reaching collimation by the spherical lens ($f = 125$ mm). A cylindrical lens ($f = 150$ mm) then focuses the light into a line that represents the intensity recorded at different viewing angles. The angle of each pixel on the ICCD array was verified by shining the beam from a HeNe laser onto a mirror placed in the object plane and rotated ± 20 deg about the centerline. The difference between the FARRS system and that used by Shirley and Winter[6] is in the addition of the reference camera in the FARRS system. The scattered signal is split before entering the iodine filter so that two separate images can be recorded, a filtered image and a reference image. Also, the observation and incident light wave vectors are oriented differently to allow the velocity and thermodynamic properties to be calculated, as discussed below.

The intensity recorded by the filtered camera is a result of the Rayleigh scattering profile combined with the filter profile and is proportional to

$$I(f_0, \Delta f_D, P, T, \theta) = \int r(f, f_0, \Delta f_D, P, T, \theta)A(f)\,\mathrm{d}f \tag{8}$$

where $A(f)$ is the transmission function of the iodine filter and r is the Rayleigh scattering profile in the frequency domain. The Rayleigh scattering profile r is given in terms of the thermodynamic properties and frequency instead of the nondimensional parameters x and y given previously. For the FARRS optical arrangement used in these experiments (Fig. 1), the Doppler shift Δf_D can be written in

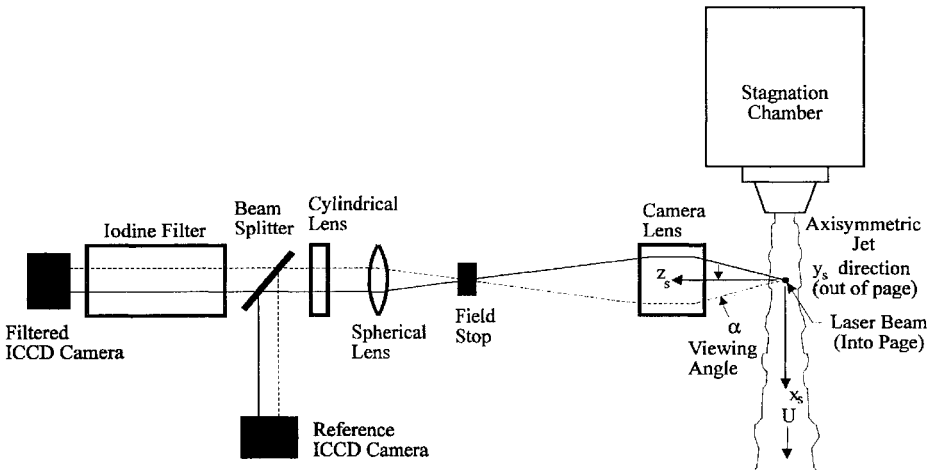

Fig. 2 Schematic of FARRS optical system.

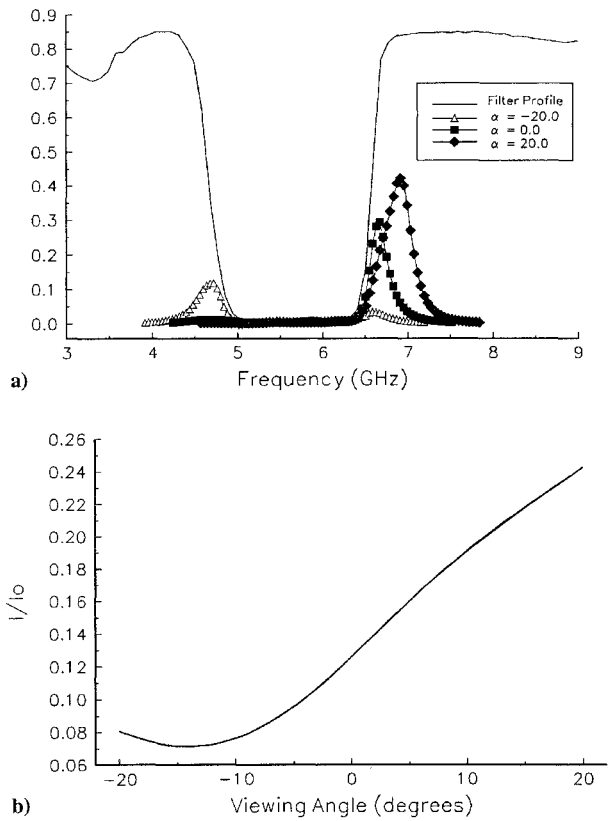

Fig. 3 Rayleigh scattering spectral profile convoluted with the iodine-filter transmission profile for: a) different viewing angles and b) the resulting intensity vs viewing-angle profile calculated from the computational model.

terms of the streamwise velocity U and viewing angle α. Therefore, the intensity is proportional to

$$I(f_0, P, T, U, \alpha, \theta) = \int r(f, f_0, U, P, T, \alpha, \theta) A(f)\, df \quad (9)$$

As given above, the position of the Rayleigh scattering profile is a function of the viewing angle and the velocity. Figure 3a gives an example of the integrand for the flow velocity and thermodynamic properties for a Mach 2 fully expanded nozzle flow (case 4 of Table 1) at three different viewing angles. (This table is discussed later.) As seen here, the Rayleigh scattering profile is shifted into and out of the absorption filter profile $A(f)$. Through integration of the profiles, the intensity vs viewing-angle profiles given in Fig. 3b are obtained.

Table 1 Run conditions for the perfectly expanded and underexpanded axisymmetric jet

Case	M_e	T_0, K	P_0, kPa	U, m/s
1	0.0	288	0.0	0.0
2	1.0	288	192	308
3	1.5	288	372	421
4	2.0	288	793	507
5	2.2	288	1000	507
6	2.3	288	1270	507

As seen in Fig. 2, a second camera records the reference image. The reference image allows the filtered image to be normalized and makes the calculation of thermodynamic quantities possible. The reference image also gives a direct measure of the density, which is proportional to the intensity of the Rayleigh scattering when no filter is used. Because the results presented in this preliminary study of the FARRS are average results, instead of using the second camera, the reference image was simply taken by removing the iodine filter and obtaining images without a filter or by tuning the laser away from the absorption line.

Experimental Arrangement

The experiments were conducted at the Aeronautical and Astronautical Research Laboratory (AARL) of Ohio State University. Figure 2 gives a schematic of the flow facility and the optical arrangement for the measurements given here. The flow used to evaluate the FARRS technique is a supersonic axisymmetric jet that exhausts into ambient air. Three nozzles with Mach numbers 1, 1.5, and 2 and an exit diameter of 19 mm were used and were operated at the conditions given in Table 1. For cases 5 and 6, the Mach 2 nozzle was operated in the underexpanded regime at the given equivalent Mach numbers (M_e, Mach number if the jet was expanded isentropically from the stagnation to ambient pressures). An air storage capacity of 41 m^3 at pressures up to 16.5 MPa allows the jet facility to be run continuously.

The interrogation laser beam is provided by a frequency-doubled (λ = 532 nm) Quanta Ray GCR-4 Nd:YAG laser, injection seeded to provide the narrow linewidth needed and a tuning range of approximately 50 GHz. With a pulse duration of 9 ns, the laser can deliver a maximum of 680 mJ of energy per pulse, although the present experiments used only a fraction of this energy (~100 mJ). The 1.0-cm-diam beam is focused down with a 1-m focal-length spherical lens to a beam waist of less than 0.1 mm. All measurements were made in the core of the jet 15 mm from the exit where the thermodynamic properties are well known, assuming isentropic flow. The Rayleigh scattering signal is collected using a Princeton Instruments 14-bit ICCD camera. McKenzie[12] showed the importance of using a high-resolution scientific-grade camera to reduce the uncertainty of the measurements. The images are stored on 486 personal computers, which provide camera

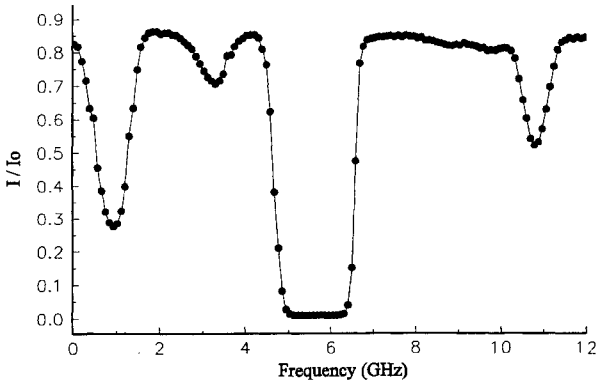

Fig. 4 FARRS iodine-filter absorption profile.

control, laser synchronization, and frequency-tuning control of the laser.

A major component of the FARRS system is the iodine filter. The iodine filter is basically a glass cylinder 9.0 cm in diameter and 22.0 cm long, with flat optical plates on both ends. Similar iodine filters have been used in other molecular filter techniques.[3–10] Iodine vapor is formed in the cell by placing a small amount of iodine crystals in the cell and evacuating it. The cell temperature (T_{cell}) is raised above the ambient temperature so that no iodine crystallizes on the windows. The cell temperature is elevated with insulated electrical heat tape and controlled with an Omega CN5052 closed-loop digital controller. The coldest point in the cell is set in a sidearm (T_{l_2}), which is housed in a water jacket and maintained at a constant temperature (±0.1°C) by a VWR circulation water bath. The temperature of the sidearm controls the vapor pressure (number density) of the iodine in the absorption cell. This method of controlling the vapor pressure has been used by other investigators.[3,10,12] The Nd:YAG laser has a narrow linewidth at a wavelength of 532 nm and can be tuned across the absorption bands of iodine. Figure 4 presents an optically thick profile of the iodine line (18787.8 cm^{-1}) used in these FARRS experiments. The profile was taken with the cell operated at $T_{cell} = 85°C$ and $T_{12} = 45°C$. Similar absorption profiles have been reported by other investigators, both experimentally and by modeling the absorption lines.[3]

Experimental Results and Discussion

Figure 5 gives the experimentally obtained images and intensity profiles for the reference camera (Fig. 5a) and the filtered camera (Fig. 5b) for the flow conditions of case 4 in Table 1. The optical effects of focusing the circular column of light through the cylindrical lens are seen in both images, resulting in a higher intensity in the center of the intensity profile. Also, the effects of the Doppler shift moving the Rayleigh scattering profile into and out of the filter are clearly seen in the filtered image as the peak intensity is shifted from the center. In the images shown, there are 200 pixels in the x_s direction, which corresponds to ±20-deg scattering angle, and 50 pixels in the y_s direction. To compare the experimental intensity profiles with those modeled by Eq. (9), the filtered image is divided by the reference image, resulting in the normalized image and intensity vs viewing-angle profile of Fig. 5c. The following profiles are based on averaging 100 single pulse images.

The first step in confirming the feasibility of the FARRS technique is to compare the experimentally measured intensity vs viewing-angle profiles with those calculated from the computational model, given the known thermodynamic conditions. Figure 6 compares the average intensity vs viewing-angle profiles for the perfectly expanded (Fig. 6a) and underexpanded (Fig. 6b) flow cases. Using the no-flow case of Fig. 6a (case 1) the FARRS system is calibrated to remove the effects attributable to optical losses, background noise, and camera intensity variations. As seen in Fig. 6, the agreement between the experimental results and the computational-model results are good. This is particularly true for the perfectly expanded cases of Fig. 6a, where the thermodynamic properties are drastically different for each case. For the underexpanded cases, there are

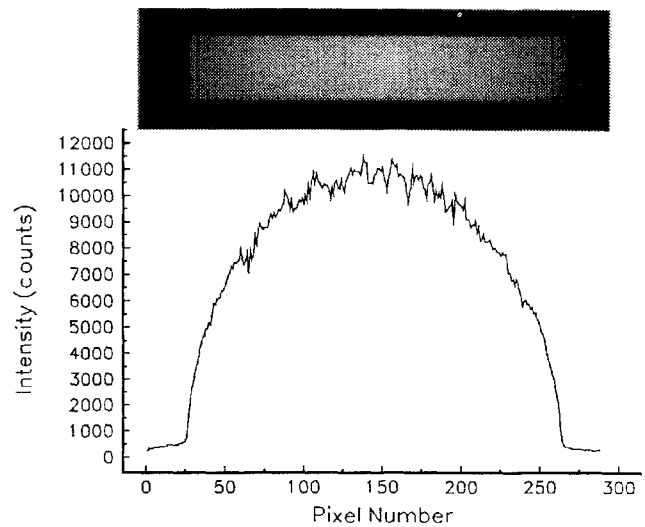

a) Reference camera

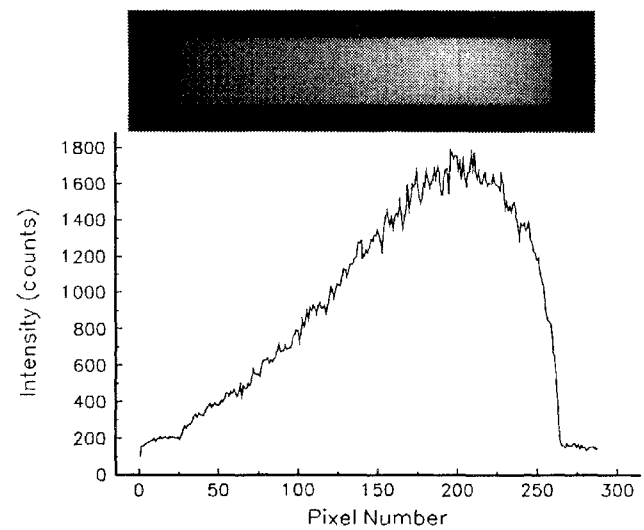

b) Filtered camera

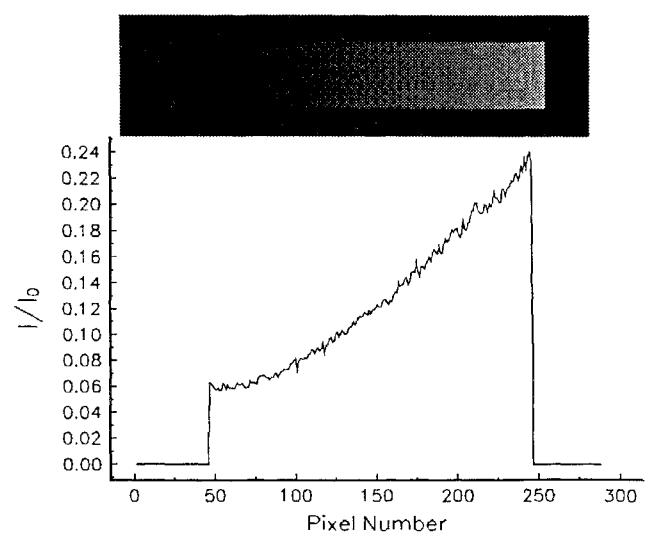

c) Resulting normalization

Fig. 5 Experimental images and profiles.

only slight changes between the profiles because the velocity for these cases is constant and the only thermodynamic change is the pressure change. The pressure modifies the shape of the Rayleigh scattering profile, which is masked when the intensity is integrated for all frequencies in the camera. Note, however, that these slight changes for the underexpanded cases are still evident in the model and the experimental results.

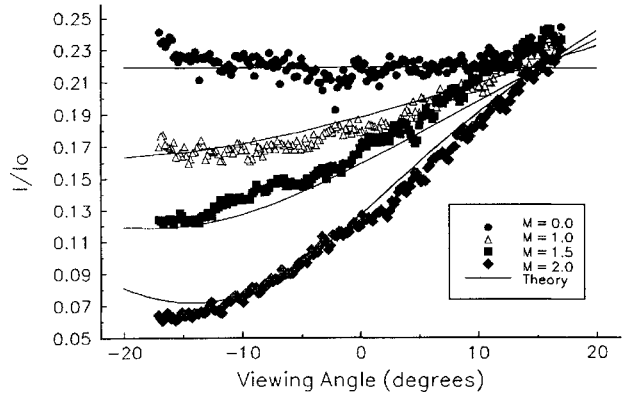

a) Perfectly expanded cases

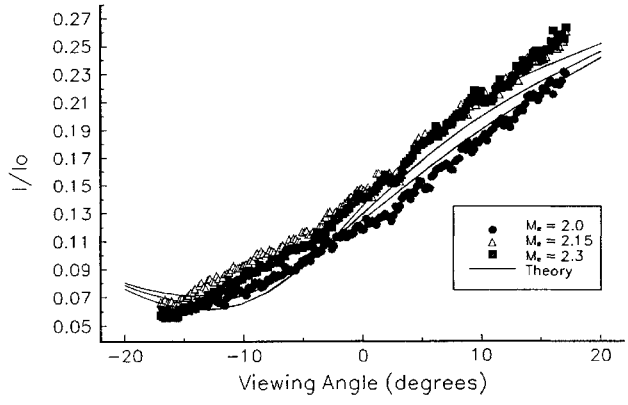

b) Underexpanded cases

Fig. 6 Experimental and computational intensity vs viewing-angle profiles.

Although the agreement of the intensity vs viewing-angle profiles is quite good between the measurements and the model, the real goal of this technique is to develop a method to simultaneously measure the velocity and thermodynamic properties when they are unknown. To accomplish this, an experimental intensity vs viewing-angle profile is obtained, and the computational model is used to back out the flow velocities and thermodynamic properties. The method is briefly described below.

First, the density is obtained directly from the reference camera because the scattered intensity with no filter is proportional to density. This can be calibrated using the no-flow case (ambient conditions) as a reference. Second, the measurements are made in the core of the jet. Because the flow velocity at the core is in the streamwise direction only, there is no Doppler shift at a viewing angle of 0 [Eq. (1)]. Therefore, the intensity at this point is not a function of streamwise velocity, and only temperature and density are needed to determine it. Using the computational model, the intensity at a 0-deg viewing angle is calculated for different temperatures and densities, as shown in Fig. 7a. Given the density and value of the experimental intensity (I/I_0) at 0 deg, the temperature can be calculated by iteratively solving the computational model. Third, from the ideal gas law, the pressure is readily attainable. Fourth, knowing these thermodynamic quantities (ρ, T, and P), the Rayleigh scattering profile is calculated for a range of velocities (Fig. 7b). The actual velocity is obtained by iteratively comparing the slope of the experimental intensity vs viewing-angle profiles with the profiles from the computational model.

Figure 8 gives the density (normalized by the ambient density ρ_{amb}), temperature, pressure, and streamwise velocities measured using FARRS, and compares them with those calculated from the isentropic flow model. The agreement is quite good for these preliminary measurements, with the measured and theoretical values differing by less than 7% for the density, temperature, and pressure and generally less than 11% for the velocity. The increased error for the velocity could be reduced by better schemes of comparing the experimental and computational profiles than using the slope alone.

Table 2 Uncertainty for velocity and thermodynamics properties

Error source	Maximum error in U%	Maximum error in T%	Maximum error in ρ%	Maximum error in P%
I	1.5	1.2	4.0	1.2
α	1.1	0.09	——	0.01
ρ	3.1	0.44	——	3.6
f_0	9.5	5.6	——	5.6
A_i	5.3	2.5	——	1.3
Total	11	5.7	4.0	6.2

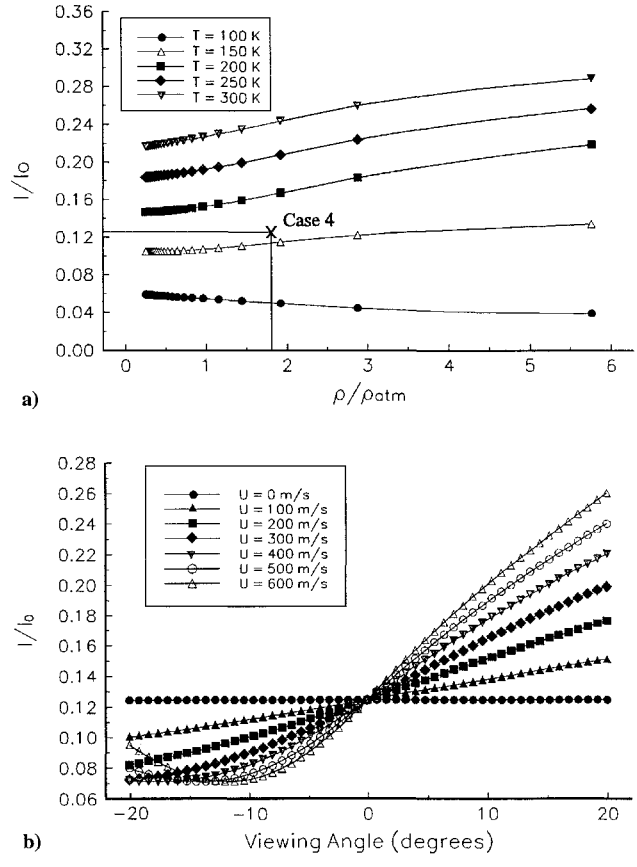

Fig. 7 Method of calculating the velocity and thermodynamic properties using: a) intensity at 0 deg viewing angle and b) intensity vs viewing-angle profile at various velocities for case 4.

Uncertainty Analysis

A simple uncertainty analysis has been performed to estimate the uncertainty associated with the thermodynamic properties and velocity measurements. The absolute error can be calculated if the property measured can be written as a function of the independent variables. Generally, the overall uncertainty is defined as

$$\Delta u_f = \sqrt{\sum_{i=1}^{n} \left(\Delta u_i \frac{\partial f}{\partial u_i} \right)^2} \tag{10}$$

where $f(u_1, u_2, \ldots, u_n)$ is the property measured as a function of the independent variables $u_1, u_2, \ldots, u_n$, which have corresponding uncertainties of $\Delta u_1, \Delta u_2, \ldots, \Delta u_n$. Although it would be ideal if one could write a closed expression for each one of the dependent variables (velocity, temperature, and pressure), this is not possible because of the computational models that are utilized in FARRS. Therefore, the partial derivatives and the total uncertainty are solved computationally using the model. The maximum uncertainties for each independent variable and the maximum total uncertainty are given in Table 2 for the cases studied here. The estimates for the uncertainty of the independent variables are ±2% for the intensity I, 0.5 deg for the viewing angle α, ±4% for the density ρ, 20 MHz

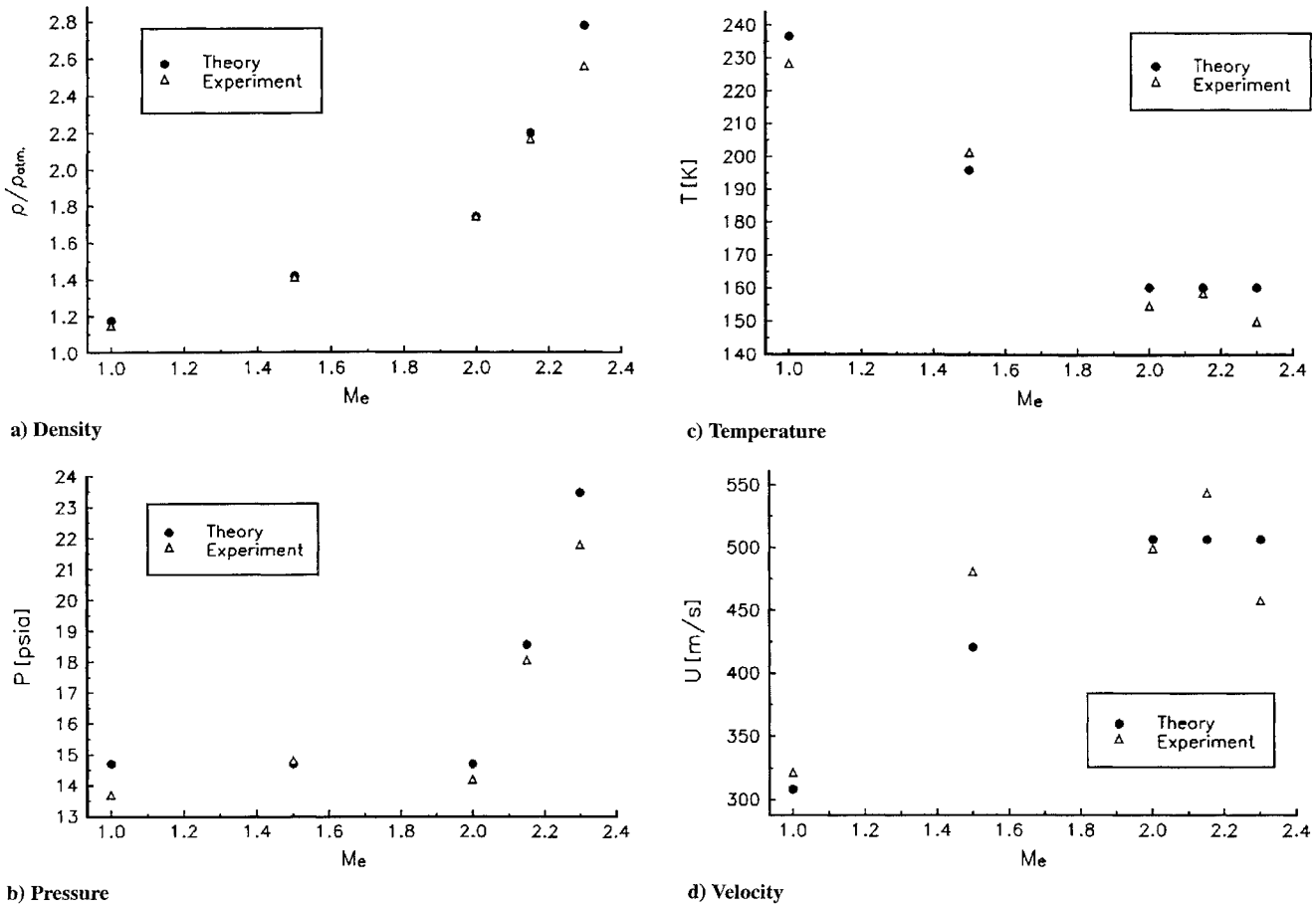

Fig. 8 Experimental and theoretical average measurements in the core of perfectly and underexpanded axisymmetric jets.

for the laser frequency f_0, 0.005 for the absorption coefficient of the filter A_i. The method of obtaining the estimates of the uncertainty of I and f_0 is given in detail by Elliott et al.[10] Note that the density is taken directly from the reference camera, and therefore, the uncertainty of 4% is attributable primarily to the laser power fluctuation and the camera noise. The uncertainty of the temperature (0.44%) and pressure (3.6%) is less than the density, however, because of the way in which the equations describing the Rayleigh scattering shape from the thermodynamic properties of the gas combine with the ideal gas law. This is clearly seen in Fig. 7, where a 4% uncertainty in the density would causes only a slight variation in the temperature. The estimate of the uncertainty in the absorption coefficient was obtained by taking multiple filter profiles and regulating the temperatures of the cell and colder sidearm which do not change over the short run times of the experiment. Although there are other possible error sources, these seem to be the dominant ones for the current technique. The total uncertainty for this preliminary study was found to be 11% for the velocity, and better than 7% for the density, temperature, and pressure, in good agreement with the experimental results.

To reduce the total uncertainty, each component should be examined individually. A major source of uncertainty is associated with the laser frequency fluctuations (f_0). Although there is current work to reduce this uncertainty in the frequency fluctuations of Nd:YAG lasers, a more practical solution is to monitor the frequency fluctuation for each instantaneous image. For example, by using a photodiode, the fluctuation in frequency could be recorded with each image by splitting off a very small portion of the laser beam and passing it through a separate molecular filter so that the nominal laser frequency would be set at the 50% absorption point. Also in this study the intensity vs viewing-angle profile was based on one row of pixels. In the future, several rows could be averaged together with only a slight loss in spatial resolution. Another area in which improvements could be made is in the scheme that compares the experimental and computational models. Currently, only three points are used to compare the curves, and the accuracy would be greatly improved using cubic spline curve-fitting routines. Incorporating these improvements should result in reducing the error to less than ±3%.

Conclusions

The feasibility of FARRS to measure average velocity and thermodynamic properties has been demonstrated in an axisymmetric jet. The computational model of the intensity profiles agree well with those measured experimentally. A method of obtaining the velocity, temperature, pressure, and density from the experimental intensity profiles, which incorporates the computational model, was proposed. The experimental measurements of the velocity and other thermodynamic properties using FARRS are within 11 and 7%, respectively. This agrees with the uncertainty calculated for the system with the highest source of error attributable to frequency fluctuations of the laser. Work is currently under way to reduce the uncertainty and extend this technique to instantaneous measurements.

Acknowledgments

The support of this research by NASA Lewis Research Center under Grant NAG3-1502 with Mark Wernet is greatly appreciated. The authors would like to thank the AARL staff and graduate students S. A. Arnette, P. S. Barry, and D. M. Milam for their help and support.

References

[1]Shimizu, H., Lee, S. A., and She, C. Y., "High Spectral Resolution Lidar System with Atomic Blocking Filters for Measuring Atmospheric Parameters," *Applied Optics*, Vol. 22, No. 9, 1983, pp. 1373–1381.

[2]Miles, R. B., Lempert, W. R., and Forkey, J., "Instantaneous Velocity Fields and Background Suppression by Filtered Rayleigh Scattering," AIAA Paper 91-0357, Jan. 1991.

[3]Miles, R. B., Forkey, J. N., and Lempert, W. R., "Filtered Rayleigh Scattering Measurements in Supersonic/Hypersonic Facilities," AIAA aper 92-3894, July 1992.

[4]Elliott, G. E., Samimy, M., and Arnette, S. A., "Study of Compressible Mixing Layers Using Filtered Rayleigh Scattering Based Visualizations," *AIAA Journal*, Vol. 30, No. 10, 1992, pp. 2567–2569.

[5]Arnette, S. A., Samimy, M., and Elliott, G. S., "Expansion Effects on Supersonic Turbulent Boundary Layers," *AIAA Journal*, Vol. 33, No. 4, 1995, pp. 430–438.

[6]Shirley, J. A., and Winter, M., "Air-Mass Flux Measurement System Using Doppler-Shifted Filtered Rayleigh Scattering," AIAA Paper 93-0513, Jan. 1993.

[7]Komine, H., Brosnan, S. J., Litton, A. B., and Stappaerts, E. A., "Real-Time Doppler Global Velocimetry," AIAA Paper 91-0337, Jan. 1991.

[8]Meyers, J. F., "Doppler Global Velocimetry: The Next Generation?" AIAA Paper 92-3897, Jan. 1992.

[9]Smith, M. W., and Northam, G. B., "Application of Absorption Filter-Planar Doppler Velocimetry to Sonic and Supersonic Jets," AIAA Paper 95-0299, Jan. 1995.

[10]Elliott, G. S., Samimy, M., and Arnette, S. A., "A Molecular Filter Based Velocimetry Technique for High Speed Flows," *Experiments in Fluids*, Vol. 18, Dec. 1994, pp. 107–118.

[11]Yip, S., and Nelkin, M., "Application of a Kinetic Model to Time-Dependent Density Correlations in Fluids," *Physical Review*, Vol. 135, No. 5A, 1964, pp. A1241–A1245.

[12]McKenzie, R. L., "Measurement Capabilities of Planar Doppler Velocimetry Using Pulsed Lasers," AIAA Paper 95-0297, Jan. 1995.